Minerals Engineering 180 (2022) 107516

Contents lists available at ScienceDirect

Minerals Engineering

journal homepage: www.elsevier.com/locate/mineng

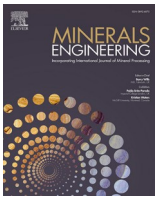

M(II)-Al-Fe layered double hydroxides synthesized from aluminum saline slag wastes and catalytic performance on cyclooctene oxidation

L. Santamaría [a], L. Oliveira García [b], E.H. de Faria [b], K.J. Ciuffi [b], M.A. Vicente [c], S.A. Korili [a], A. Gil [a,*]

[a] INAMAT^2-Departamento de Ciencias, Edificio de los Acebos, Universidad Pública de Navarra, Campus de Arrosadía, E-31006 Pamplona, Spain
[b] Grupo de Pesquisas em Materiais Lamelares Híbridos (GPMatLam), Universidade de Franca, Av. Dr. Armando Salles Oliveira, 201, Parque Universitário, 14404-600 Franca, SP, Brazil
[c] GIR-QUESCAT, Departamento de Química Inorgánica, Facultad de Ciencias Químicas. Plaza de los Caídos s/n. 37008, Universidad de Salamanca, Salamanca, Spain

ARTICLE INFO

Keywords:
Aluminum industrial wastes
Hydrotalcite
Iodosylbenzene
Saline slags
(Z)-cyclooctene oxidation

ABSTRACT

Aluminum was extracted from saline slags via an alkaline method and employed in the synthesis of Layered Double Hydroxides (LDH) with various M^{2+} cations (Co, Mg, Ni and Zn), while Al and Fe were the M^{3+} cations, using the co-precipitation method and a M^{2+}/M^{3+} 2:1 ratio. The structural characterization of the samples was performed with powder X-ray diffraction (PXRD), scanning electron microscopy (SEM), nitrogen physisorption at 77 K, thermogravimetric analysis (TGA), temperature-programmed reduction (TPR) and X-ray photoelectron spectroscopy (XPS). Their catalytic performance was tested for the oxidation of olefins (cyclooctene) and their biomimetic potential was analyzed. Results show a great selectivity towards epoxides with no other products obtained. Reaction yields followed the descending order Co_4AlFe, Zn_4AlFe, Ni_4AlFe, and Mg_4AlFe, the sample with cobalt as M^{2+} converting up to 85% of cyclooctene.

1. Introduction

Although the aluminum recycling process is carried out without the loss of quality in the final product and saves between 80 and 95% of the energy needed in the primary production (Gil, 2005), the use of salt fluxes in order to obtain better performances produces an undesirable and hazardous waste during this process (European Commission, 2014), saline slags (waste code 100308*). Finding direct applications for the slags such as inert filling for construction or road paving has been studied (Gil and Korili, 2016; Javali et al., 2017) as it can reduce the controlled landfill management costs although it also implies environmental risks (Lin et al., 2021). Another much interesting option, chosen in this work, is the extraction of the aluminum still present in the slag and the synthesis of an added-value product with a direct application as a heterogeneous catalyst.

Layered double hydroxides (LDH), also called hydrotalcite-like compounds as they mimic the structure of hydrotalcite $Mg_6Al_2CO_3(OH)_{16}{\cdot}4H_2O$, are formed from an octahedral framework similar to brucite ($Mg(OH)_2$) with a substitution of some of the M^{2+} for M^{3+} cations. This change generates an overall positive charge in the structure that is compensated by the placement of anions in the interlayer. Multiple combinations of various M^{2+}, M^{3+} and anions can be used which confer the LDH several characteristics and gives this family of clays multiple applications: as catalysts (Qiu et al., 2019), adsorbents (Jawad et al., 2019), in medicine (Asif et al., 2018), photochemistry (El Hassani et al., 2019; Trujillano et al., 2020) or electrochemistry (Qiu et al., 2019). This is due to several characteristics such as easy-to-tailor properties or high versatility: LDH can be designed to fulfil specific requirements (Li and Duan, 2005). The use of LDH as catalysts gives the advantage of having a high degree of dispersion of the transition metal in the catalytic structure. Many works have been reported on the use of non-calcined LDH in catalytic reactions: the epoxidation of styrene by MgAl LDH (Kirm et al., 2004), the hydroxylation of phenol by CoNiAl LDH (Rives et al., 2003) or the carbonylation of methanol by NiAl LDH (Kapoor and Matsumura, 2004). However, the mixed metal oxides obtained by thermal decomposition of the LDH are usually the preferred choice for the catalysts (Ahmed et al., 2012; Lee et al., 2021) as they have large specific surface areas (up to 300 m^2/g), basic properties, a thermally stable dispersion of the metal ions and the possibility of synergetic effects between the elements.

* Corresponding author.
E-mail address: andoni@unavarra.es (A. Gil).

https://doi.org/10.1016/j.mineng.2022.107516
Received 18 January 2022; Received in revised form 25 February 2022; Accepted 18 March 2022
Available online 25 March 2022

Recent technological advances combined with the need for new functions have increased the demand for new materials with multiple functions. In order to improve the industrial applicability of the LDH-based nanocomposites prepared here, their catalytic potential in the oxidation of cyclooctene by iodosylbenzene was tested. Although LDH is known for the presence of basic sites, proven here, the presence of iron ions in the LDH-based catalytic materials could generate acid sites and enhance their application in oxidation reactions, not to mention that iron is known to be the active species in these reactions, mimicking biological enzymes such as cytochrome P450. To confirm the possible biomimetic potential of the LDH-based catalytic materials prepared herein, cyclooctene was selected as substrate: it generally affords cyclooctene oxide as the main product, and epoxides are useful and expensive intermediates for chemical and pharmaceutical industries. Thus, cyclooctene was chosen as a "diagnostic substrate" to determine the catalytic activity of a new material (Antonangelo et al., 2017; Bizaia et al., 2009; Caetano et al., 2006).

In the present work, the preparation, characterization and catalytic oxidation behavior of a series of LDH prepared with Al^{3+} extracted from saline slags is reported. The presence of Fe^{3+} together with Al^{3+} and the possible synergic effect of its presence, together with that of cobalt, zinc, nickel and magnesium as divalent cations, was tested on the catalytic performance of the catalysts on the (Z)-cyclooctene epoxidation to cyclooctene oxide by iodosylbenzene.

2. Experimental procedure

2.1. Materials

The synthesis of hydrotalcites was performed using $Co(NO_3)_2{\cdot}6H_2O$ (Panreac, ≥ 98%), $Mg(NO_3)_2{\cdot}6H_2O$ (Sigma-Aldrich, ≥ 99.99%), $Ni(NO_3)_2{\cdot}6H_2O$ (Panreac, ≥ 98%), $Zn(NO_3)_2{\cdot}6H_2O$ (Sigma-Aldrich, ≥ 98%), $Fe(NO_3)_3{\cdot}9H_2O$ (Riedel de Häen, ≥ 96%) and Na_2CO_3 (Sigma-Aldrich, ≥ 99.99%). HNO_3 was used for pH adjustment and NaOH (Panreac) for both pH adjustment and aluminum extraction (see next section). (Diacetoxyiodo)benzene (Sigma-Aldrich, 98%), (Z)-cyclooctene (Sigma-Aldrich, 98%) and dichloroethane (ACS reagent, ≥99.0%) were used for the oxidation reaction, being used as received, without any modification.

2.2. Hydrotalcite-like compounds synthesis

Aluminum was obtained from the saline slag by an alkaline extraction process: 5 g of the slag were added to 100 mL of a NaOH 2 mol/L solution, it was placed in a reflux system stirred at 500 rpm and at a temperature of 373 K during 1 h. Filtration was used to separate the slurries, and the aluminum present in the filtrated solution was 6.15 (±) 0.14 g/L (or 0.23 (±) 0.005 mol/L), determined by ICP-OES. Along with aluminum, small quantities of other metals such as iron, calcium or magnesium are also extracted, a more detailed description of the chemical composition of the slag before and after aluminum extraction can be found in previous publications of our groups (Santamaría et al., 2022; Yoldi et al., 2019).

The LDH were synthesized by the co-precipitation method, with an atomic ratio of M^{2+}:(Al, Fe)$^{3+}$ 2:1. Four samples were synthesized with the same ratio and changing the M^{2+} (Co, Mg, Ni and Zn were used). As an example, 0.08 mol/L of $Ni(NO_3)_2{\cdot}6H_2O$, 0.02 mol/L of Fe $(NO_3)_3{\cdot}9H_2O$ and aluminum from the extraction, slightly diluted (0.02 mol/L) were added dropwise to a 0.015 mol/L solution of Na_2CO_3 to a total volume of 0.4 L. The synthesis pH was continuously adjusted to 10 by using both NaOH and HNO_3 as needed. The mixture was stirred at 500 rpm and 333 K for 1 h and then left to age for 24 h. Milli-Q water was employed to wash the samples and they were then centrifuged (8000 rpm, 5 min) as many times as needed until the pH lowered to 7. All materials were dried for 353 K and 16 h and manually grounded with a mortar. Samples were named by their stoichiometric proportions as Co_4AlFe, Mg_4AlFe, Ni_4AlFe or Zn_4AlFe, respectively.

2.3. Characterization techniques

Powder X-ray diffraction (PXRD) diagrams were recorded on a Siemens D-5000 instrument using a Ni-filtered Cu Kα radiation (λ = 0.15418 nm) in a 2θ range from 5 to 70° and a 0.2° (2θ)/min scanning rate. The working current of the X-ray source was 30 mA and the voltage 40 kV. The software Diffract-AT was used to analyze the patterns and the identification of the crystalline phases present in the samples was performed by comparison with the JCPDS diffraction files (ICDD database).

Scanning electron microscopy (SEM) was used to analyze the morphology of the samples on a Phenomenom World, XL operating at 15 kV.

Specific surface area and porosity of the samples was evaluated at 77 K with a Micromeritics ASAP 2020 Plus adsorption analyzer. The samples (0.4 g) were outgassed before measurement, under vacuum at 423 K for 24 h. The specific surface area (S_{BET}) was evaluated by the BET method in the range between 0.05 and 0.20 of relative pressure. The total pore (Vp) and micropore volumes ($V\mu p$) were also calculated using the Gurvitsch and the *t-plot* methods.

The thermogravimetric measurements (TG) were recorded in a Hi-Res TGA2950 apparatus (TA-Instruments). The samples were heated up from room temperature to 1173 K with a 10 K/min heating rate under a dry air atmosphere (60 mL/min).

Temperature-programmed reduction (TPR) runs were performed on a Micromeritics TPR/TPD 2900 instrument from Micromeritics under a 30 mL/min flow of 5% H_2 (H_2/Ar, Praxair) carrier gas to reduce the samples. The gas at the reaction exit was passed through a cold trap (melting isopropanol) to retain vapors and condensable gases formed during the precursor decomposition, before entering the detector.

X-ray photoelectron spectra (XPS) were recorded using a SSX 100/206 spectrometer for Surface Science Instruments (USA) equipped with a monochromatized and microfocused Al X-ray source powered with 20 mA and 10 kV. The pressure within the analysis chamber was around 10^{-6} Pa. The zone analyzed was around 1.4 mm^2, and the pass energy was set to 150 eV for the general spectra and to 30 eV for the elementary spectra. An electron gun set at 8 eV and the charge was stabilized with a nickel grid placed 3 mm above the surface of the samples. The surface adventitious carbon peak, C 1 s at 284.8 eV, was used as a reference for all the binding energies.

2.4. Catalytic performance

Iodosylbenzene (PhIO) was collected for the first time by hydrolysis of iodosylbenzene diacetate (Sharefkin and Saltzmann, 1963), iodometric titration was employed to test the purity of the compound obtained (Lucas et al., 1963). Iodosylbenzene (0.023 mmol) was added to a 4 mL vial sealed with a teflon-coated silicone septum containing Co_4AlFe, Mg_4AlFe, Ni_4AlFe or Zn_4AlFe (10 mg); 1,2-dichloroethane (1 mL); (Z)-cyclooctene (previously purified on alumina column) (1.15 mmol); and di-n-butyl ether as internal standard (5 μL). The mixtures were kept under magnetic stirring at room temperature, the reaction was followed for 96 h, with aliquots extracted and analyzed at several times: 4, 6, 12, 24, 48, 72 and 96 h. A HP 6890 gas chromatograph was employed to analyze the reaction products using a hydrogen flame ionization detector and a capillary column (HP-INNOWax-19091 N-133, polyethyleneglycol length = 30 m, internal diameter = 0.25 μm). The products were quantified using a calibration curve obtained with a standard solution and the yields were based on added oxidant (iodosylbenzene). All the reactions were performed in triplicate. In all cases, a control of the reaction was carried out in the absence of catalyst.

At the end of the tests for (Z)-cyclooctene oxidation, the catalysts were recovered by centrifugation and washed 5 times with 1 mL methanol to ensure that any remaining iodosylbenzene was removed from the catalyst. The catalysts were then dried for 3 h at 333 K, before

being used again.

3. Results and discussion

3.1. Characterization of the catalysts

Fig. 1**a and 1b** show the powder XRD patterns of the samples. The crystallographic phases present on the fresh LDH (dried at 353 K, Fig. 1**a**) show single-phase materials with the $3R_1$ polytype and the general formula $M_4Al_2CO_3(OH)_{12}{\cdot}4H_2O$. Although in some cases the segregation of hydroxides or oxides can occur and be quantified (Misol et al., 2020), the reflections show that the samples have very few to no side products with samples having different peak intensities. These peaks increase as we move right on the Periodic Table and even though a bigger sharpness in the peaks cannot be directly correlated to an enhancement in the sample crystallinity because of phenomena such as constructive interference, a large increment in sharpness is expected to correlate with crystallinity refining (Naseem et al., 2019). The crystallite sizes of the four samples were calculated from the most intense diffraction peak (0 0 3) of hydrotalcite phase, placed at 11°, with the Scherrer equation:

$$\tau = \frac{K\lambda}{\beta_\tau cos\theta}$$

where K is the shape factor = 0.9; $\beta\tau$ is the width of the peak at half of the maximum intensity (FWHM) after subtraction of instrumental broadening and θ is the diffraction angle. Zn_4AlFe LDH pattern is best defined

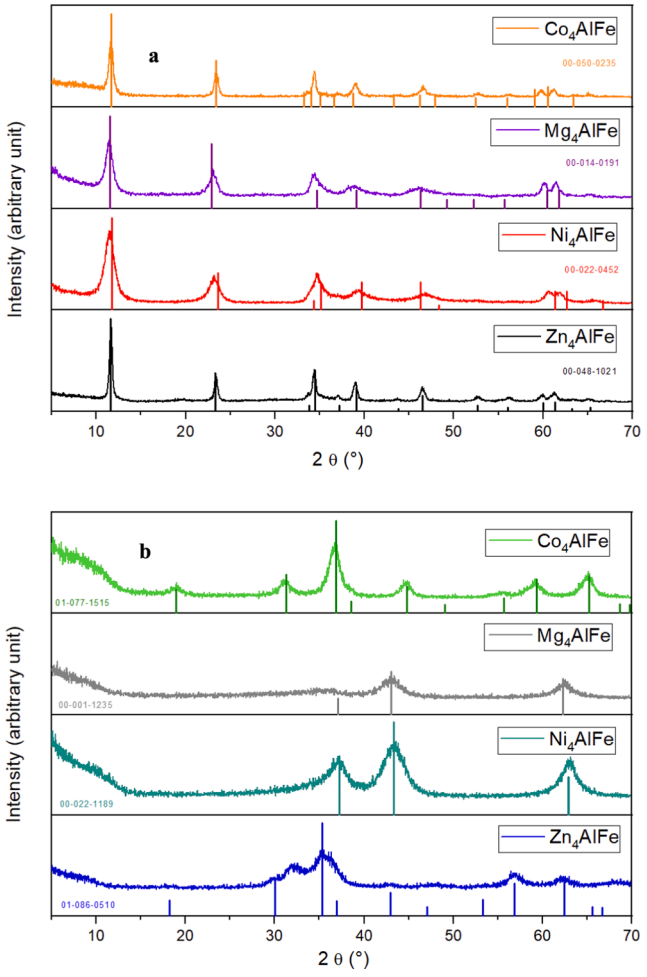

Fig. 1. Powder X-ray diffraction (PXRD) patterns of non-calcined (a) and calcined samples (b).

than the other three samples and has at least the double of crystallite size (see Table 1). Samples in the descending order Zn > Co > Mg > Ni show similar trend to LDH samples with no Fe in their composition (Santamaría et al., 2020a). c parameter was calculated from the d-spacing of the samples from the d_{003} and d_{006} reflections located at $2\theta \approx 11.6$ and 23.3° using Bragg's equation. It is related to the interlayer distance representing three times the basal spacing and was determined with the formula $c = 3/2(d_{003} + 2d_{006})$. The results are shown in Table 1: the interlayer space is close to 0.3 nm (as the thickness of the brucite layers is 0.48 nm (Cavani et al., 1991)) and no significant differences are shown as all the samples have carbonate anions with their molecular plane parallel to the brucite-like layers (Fernández et al., 1998). The lower value of Co_4AlFe sample indicates that carbonate anions are involved in stronger intermolecular interactions in this sample (Chagas et al., 2015). The average distance between cations is seen with a parameter, calculated $a = 2d_{(110)}$. The increased distance correlates with the ionic radius of M^{2+} and a general shift to lower 2θ values is observed when compared to LDH samples with only aluminum as M^{3+} (Santamaría et al., 2020a) suggesting an introduction of Fe^{3+} in the LDH structure in octahedral coordination (ionic radius = 0.645 nm), which is bigger than Al^{3+} (ionic radius in octahedral coordination = 0.535 nm) (Greenwood and Earnshaw, 1997). The attempts to introduce Fe^{3+} in the structure of LDH have been previously successful, however with the increment of Fe^{3+} content a limit is reached after which iron does not enter the brucite structure. This does not show as new peaks in the form of iron oxide or oxohydroxide because of its low percentage but can be observed as a noticeable decrease in the intensities of the peaks (Parida et al., 2012), something that cannot be seen when comparing our samples with those without iron (Santamaría et al., 2020a), thus indicating that a good substitution degree was achieved.

The calcination of the samples at 673 K for 4 h (Fig. 1**b**) led to the removal of the volatile carbonates and water from the interlayer and the hydroxyl groups, and the corresponding divalent oxides $M^{2+}O$ were formed, except in the case of cobalt where Co_3O_4 was detected. The presence of other $M^{2+}M^{3+}{}_2O_4$ spinels could not be confirmed as they usually appear after calcination at higher temperatures, depending on the metal cations involved, although small traces of $MgFe_2O_4$ have been detected from 723 K (Fernández et al., 1998).

The micrographs of the calcined samples are shown in Fig. 2 where the layered structure can be deduced especially from Fig. 2**a**. A small proportion of silicon (<1% atomic) is found by the EDX analysis which is something to be expected. Even though the alkaline aluminum extraction process of the slag is more selective than the acid procedure, which dissolves other unwanted metals, a small proportion of silicon is usually extracted along with the aluminum (Murayama et al., 2012; Yoldi et al., 2019).

The specific surface area of the four samples, fresh and calcined, as determined from the nitrogen adsorption isotherms at 77 K can be seen in Table 2. The isotherms, shown in Fig. 3 (**3a** for uncalcined and **3b** for calcined samples), belong to type II and correspond to unrestricted adsorption and do not show the layered structure of the solids, as the nitrogen molecules are not capable of entering the interlayer space (0.3 nm) that is already filled with water and carbonate anions (Hernández et al., 2017). The specific surface area values for the uncalcined samples go from 88 and 91 m^2/g of Co_4AlFe and Zn_4AlFe to 122 and 155 m^2/g of

Table 1
Diffraction spacings (see Fig. 1), crystallite size, and c and a parameters of the non-calcined layered double hydroxides (LDH) samples.

Sample	$d_{(003)}$	$d_{(006)}$	$d_{(110)}$	c (nm)	a (nm)	Crystallite size (nm)
Co_4AlFe	0.759	0.380	0.155	2.280	0.3104	16.38
Mg_4AlFe	0.778	0.385	0.154	2.323	0.3085	7.93
Ni_4AlFe	0.774	0.385	0.153	2.315	0.3067	6.34
Zn_4AlFe	0.762	0.382	0.155	2.290	0.3096	29.84
Mg_4Al_2 Reference code: 01–070-2151				2.281	0.3054	–

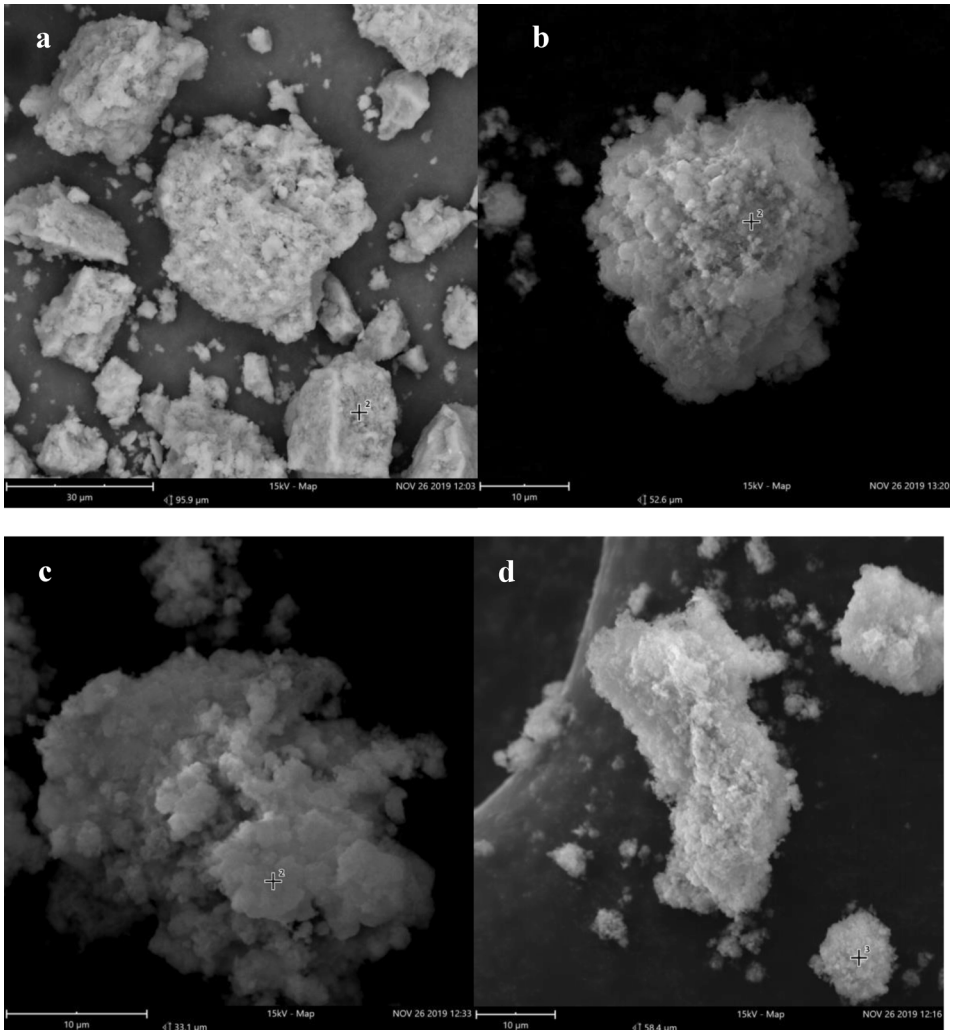

Fig. 2. Scanning electron microscopy (SEM) micrographs of the cobalt (a), magnesium (b), nickel (c) and zinc (d) samples.

Table 2
Textural properties of the non-calcined and calcined layered double hydroxides (LDH) samples.

Sample	S_{BET} (m^2/g)	V_p (cm^3/g)	$V_{\mu p}$ (cm^3/g)
Co_4AlFe (423 K)	88	0.458	0.005
Co_4AlFe (673 K)	124	0.606	–
Mg_4AlFe (423 K)	122	0.413	0.006
Mg_4AlFe (673 K))	202	0.677	0.004
Ni_4AlFe (423 K)	155	0.694	0.007
Ni_4AlFe (673 K))	195	0.894	0.007
Zn_4AlFe (423 K)	91	0.369	0.002
Zn_4AlFe (673 K))	78	0.417	0.003

Mg_4AlFe and Ni_4AlFe. The calcination of the samples at 673 K brings the end of the layered structure (as seen in the PXRD analysis) and this usually means an increase in the surface area value of the samples, which actually occurs in all samples but Zn_4AlFe, where the specific surface area decreases from 91 to 78. This behavior has been described before in LDH with a zinc:aluminum ratio of 3:1 (Hadnadjev-Kostic et al., 2013; Santamaría et al., 2020b) due to a different response to calcination. These results show that the crystallinity of the samples is responsible for these values. The more amorphous a sample is, the bigger its specific surface area when calcined (Fernández et al., 1998), as can be seen in the sharpness of the peaks in Fig. 1 and the crystallite size from Table 1.

Representative thermogravimetric (TG) and derivative thermogravimetric (DTG) curves for the samples are shown in Fig. 4. Mass loss stars at room temperature and is completed at around 900 K. There are different steps which show minor mass loss differences between the samples, shown in Table 3. The first step, up to 400 K, comes from the loss of adsorbed water and gases. The second step goes up to 500 K and represents around a 10 % of mass loss which corresponds to the interlayer water. In the third step the biggest differences between the samples are displayed, it shows another large mass loss which can go from up to 550 K with an 8.9 % decrease in the case of Co_4AlFe to up to 700 K and a 20.5 % mass loss in the case of Mg_4AlFe. The last steps are minor and correspond to the formation of mixed metal oxides (step 4) and the sintering process starting point (step 5) that causes a collapse of the pores. A variation of the equation taken from (Naseem et al., 2019) was employed to calculate the difference in mass losses from the theoretical values, considering that water and carbon dioxide exit the system:

$$\left\{M_{(1-x)}Fe_{x/2}Al_{x/2}(OH)_2\right\}\bullet\left\{CO_{3\frac{x}{2}}\cdot nH_2O\right\}\xrightarrow{\Delta}(1-x)MO\bullet x/4Fe_2O_3\cdot x/4Al_2O_3+yH_2O+x/2CO_2$$

Table 4 shows a comparison between the expected and experimental mass loss results. The atomic masses of the M^{2+} are responsible for the difference between the samples. The variance from the theoretical values is minor except in the case of Zn_4AlFe sample where a 6.5 % extra

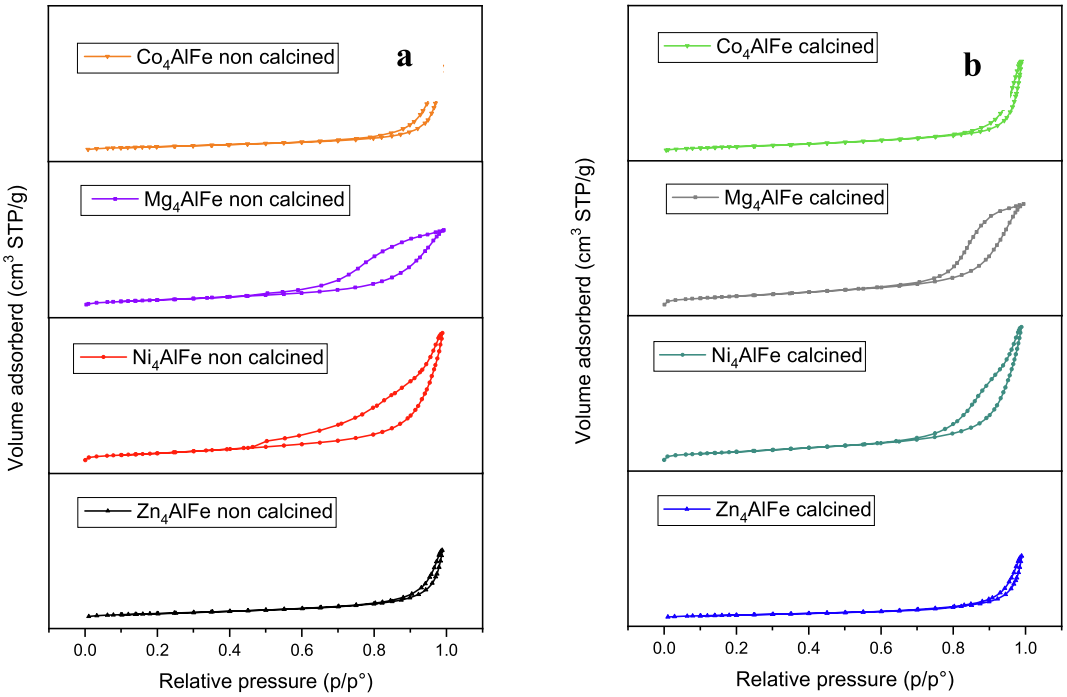

Fig. 3. Nitrogen adsorption–desorption isotherms of non-calcined (a) and calcined (b) series of layered double hydroxides (LDH) samples.

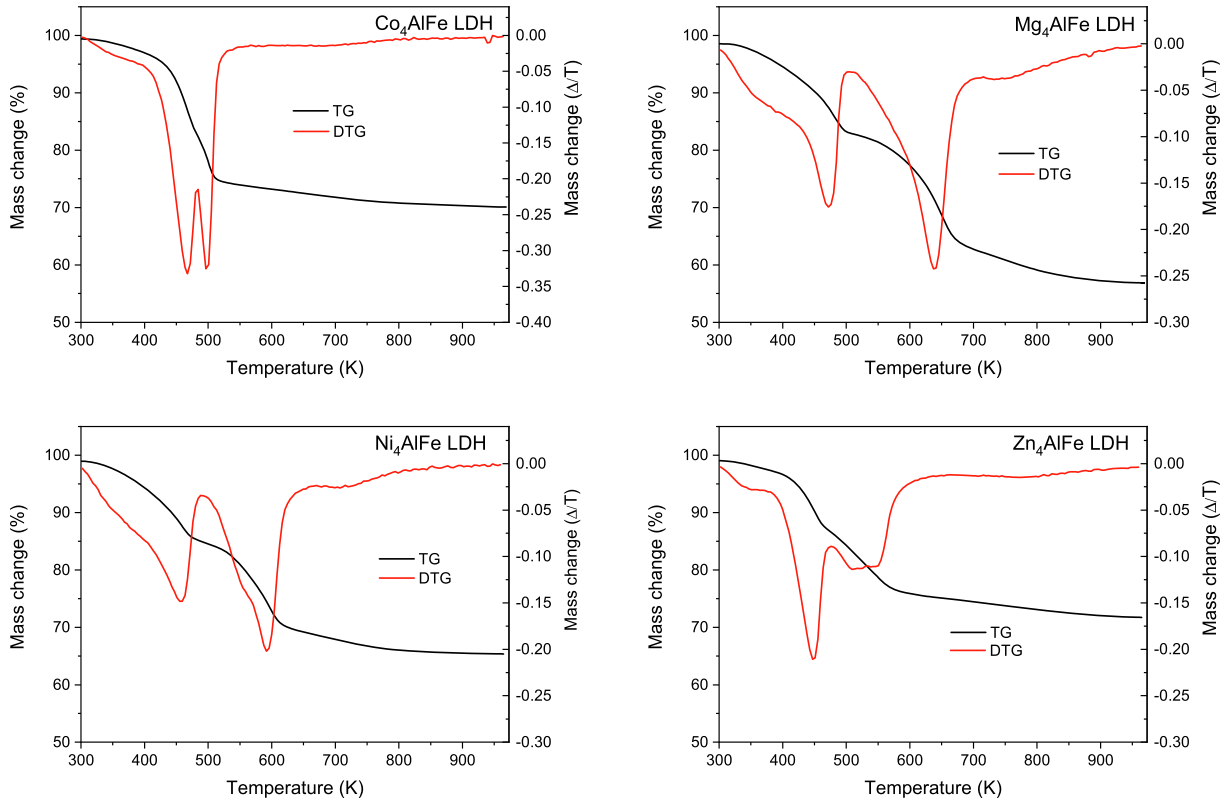

Fig. 4. Thermogravimetric (TG) and derivative thermogravimetric (DTG) curves of the layered double hydroxides (LDH) prepared with extracted aluminum.

mass is left.

The four calcined samples were subjected to a temperature-programmed reduction (TPR) process with H_2 up to 1100 K and the TCD output is displayed in Fig. 5. Mg_4AlFe sample can be used as a reference for the iron content of the samples as a calcined hydrotalcite with only magnesium and aluminum gives little to no signal in TPR analysis (Santamaría et al., 2020a). The first peak at about 720 K is related to the reduction of Fe_2O_3 to Fe_3O_4 and the second peak, a combination of the reduction of Fe_3O_4 to FeO and that to Fe can be found from 850 K and ends out of the range of this analysis (Webb and Orr, 1997). The signal from Zn_4AlFe solid seems to be a convolution of the three peaks. Both Co_4AlFe and Ni_4AlFe have added peaks due to their

Table 3
Mass losses (wt.%) in the steps indicated from the thermogravimetric analyses of the layered double hydroxides (LDH) samples.

Step → Sample ↓	1	2	3	4	5	TOTAL (mass loss wt.%)
Co_4AlFe	300–400 K	400–480 K	480–550 K	550–750 K	750–1000 K	
	3.1 %	14.0 %	8.9 %	2.8 %	1.1 %	29.9 %
Mg_4AlFe	300–400 K	400–500 K	500–700 K	700–800 K	800–1000 K	
	5.7 %	11.2 %	20.5 %	3.6 %	2.2 %	43.2 %
Ni_4AlFe	300–400 K	400–500 K	500–650 K	650–800 K	800–1000 K	
	5.9 %	9.7 %	15.4 %	3.1 %	0.7 %	34.6 %
Zn_4AlFe	300–375 K	375–475 K	475–650 K	650–850 K	850–1000 K	
	2.6 %	11.0 %	11.4 %	2.6 %	0.7 %	28.3 %

Table 4
Comparison of the theoretical and measured remaining mass of the layered double hydroxides (LDH) samples.

LDH	Theoretical oxides structure	Theoretical remaining mass (%)	Measured remaining mass (%)	Variance from theoretical value (%)
$Co_4AlFeCO_3(OH)_{12}{\cdot}4H_2O$	$4/3Co_3O_4 + Al_2O_3 + Fe_2O_3$	69.0	70.1	1.5
$Mg_4AlFeCO_3(OH)_{12}{\cdot}4H_2O$	$4MgO + Al_2O_3 + Fe_2O_3$	57.9	56.8	0.4
$Ni_4AlFeCO_3(OH)_{12}{\cdot}4H_2O$	$4NiO + Al_2O_3 + Fe_2O_3$	65.7	65.4	−0.5
$Zn_4AlFeCO_3(OH)_{12}{\cdot}4H_2O$	$4ZnO + Al_2O_3 + Fe_2O_3$	67.1	71.7	6.5

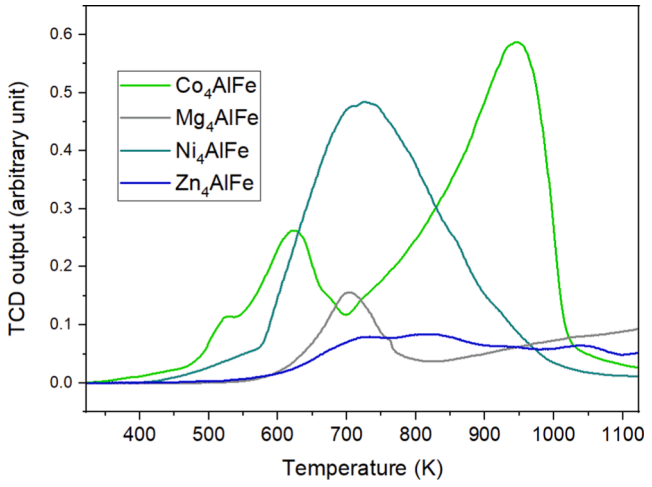

Fig. 5. H_2-temperature-programmed reduction (TPR) profile of Co_4AlFe, Mg_4AlFe, Ni_4AlFe and Zn_4AlFe calcined samples.

M^{2+} reduction capacity, and in the first case the reduction effects are increased by the oxidation of cobalt during the calcination process. Thus, Ni_4AlFe has a peak with a maximum at 725 K that corresponds to the change from NiO to Ni in which the reduction of Fe is included, while Co_4AlFe shows two peaks at 600 K (from Co_3O_4 to CoO) and 950 K (from CoO to Co). The reduction of Fe_2O_3 to Fe_3O_4 can be seen here at 700 K as the signal does not reach the baseline between the peaks.

XPS analysis were performed to analyze the surface concentrations of the metals in the four different samples. Table 5 shows the surface concentrations (% atomic) and relative proportion of metals in the calcined samples. The relative proportion of aluminum in three of the samples could be due to its smaller mass, which make it easier to migrate to the surface as the calcination process occurs (Li et al., 2009). The proportions of iron in the surface of the samples could be partly responsible for the different results of the calcinated samples performances; as will be shown in the next section, as the proportion of iron descends, so does their cyclooctene oxide yield.

Table 5
Surface concentration (% atomic) and metals proportions on the calcined layered double hydroxides (LDH) samples.

Surface concentration (% atomic)	M^{2+}	Al	Fe	O	C	Proportions of metals
Co_4AlFe	17.3	6.6	5.0	57.8	13.2	$Co_4Al_{1.5}Fe_{1.2}$
Mg_4AlFe	19.0	5.2	3.7	58.3	13.8	$Mg_4Al_{1.1}Fe_{0.8}$
Ni_4AlFe	21.6	5.6	5.0	53.4	14.3	$Ni_4Al_1Fe_1$
Zn_4AlFe	17.6	5.1	3.6	51.2	22.5	$Zn_4Al_{1.2}Fe_{0.8}$

3.2. Catalytic performance

PhIO was chosen as oxygen source because it has traditionally been employed in oxidation reactions involving cytochrome P450 biomimetic systems based on metalloporphyrins or transition metals as catalysts (Antonangelo et al., 2017; Bizaia et al., 2009; Caetano et al., 2006); it produces good oxidation conversion; it is relatively inert in the absence of catalysts; it may react with biomimetic catalysts to generate high-valent oxo-metal species; and its use prevents the free radical chain reactions that are normally initiated by oxidants like alkyl hydroperoxides (R-O-O-H) (Caetano et al., 2006; Groves, 2006).

Fig. 6**a** shows the results for cyclooctene oxidation catalyzed by the LDH-based catalytic materials without heat-treatment. All the tested materials selectively catalyzed cyclooctene oxidation to cyclooctene oxide (epoxide), the sole product. The overall accountability for the oxidant was achieved by measuring the iodobenzene (PhI) yield in all the reactions, to find that PhIO was totally consumed, and that the PhI yields were *ca.* 100%. Therefore, all the oxidant was converted to PhI, and the competitive reaction between the active intermediate and another PhIO molecule, to form $PhIO_2$, did not occur.

As expected for heterogeneous systems, longer reaction times provided better yields because substrate access to and product diffusion from the active site was facilitated. In general, the best yields start to be attained after 24 h of reaction for all the LDH-based catalytic materials. For comparison purposes, controls were carried out for all the reactions in the absence of catalytic material and in the presence of LDH. The control reactions in the absence of iron did not show detectable substrate oxidation, and that reactions in the absence of oxidant did not yield any product.

The epoxide yields obtained followed the descending order: Co_4AlFe, Zn_4AlFe, Ni_4AlFe, and Mg_4AlFe. The LDH-based catalytic material Co_4AlFe gave 54% epoxide yield while the other three samples showed similar performances with an epoxide yield between 15 and 18%. As also seen on a previous work on kaolinite (Bizaia et al., 2009), surface area and catalytic results were not related.

To understand the effect of metals on the catalytic process, the LDH-based catalytic materials were heat-treated at 673 K for 4 h (Fig. 6**b**). Epoxide yields increased with respect to the uncalcined solids, and the

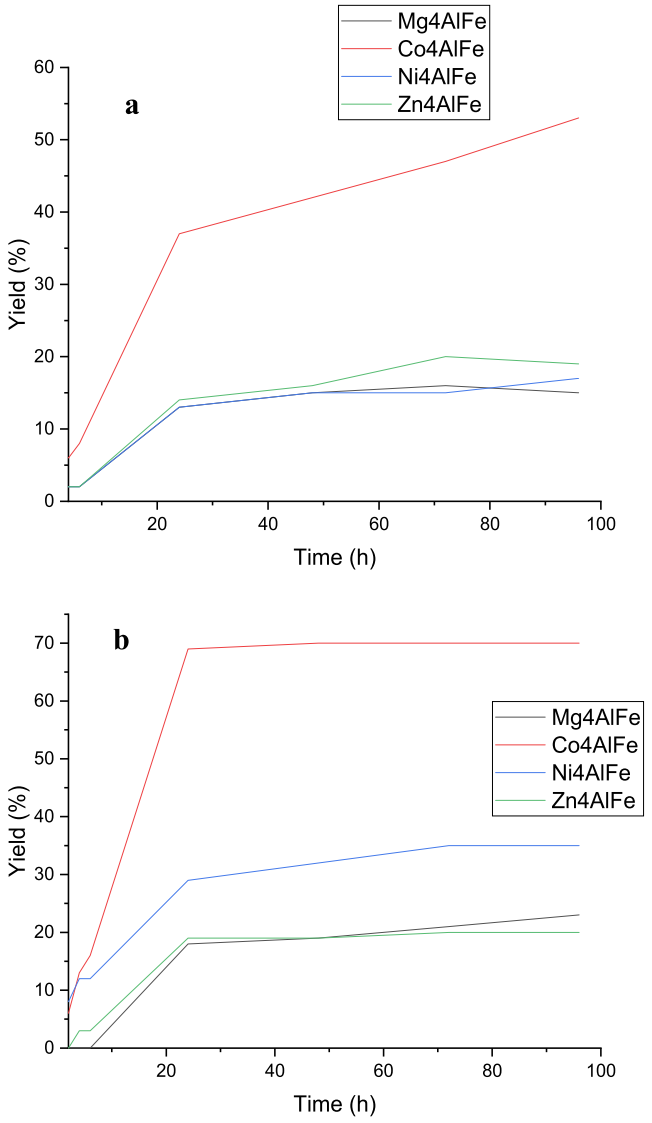

Fig. 6. Oxidation of cyclooctene using catalysts without thermal treatment (a) and after thermal treatment at 673 K for 4 h (b).

relative order of activity among the different solids changed, finding for the calcined solids the following descending order, Co_4AlFe, Ni_4AlFe, Mg_4AlFe, and Zn_4AlFe, with heat-treated LDH-based Co_4AlFe solid providing 70 % epoxide yield. When results were compared to the data in Table 2, no direct relation was found between catalyst surface area and epoxide yield, but heat-treatment increased the surface area and pore size of the LDH-based catalytic materials, improving exposure of the active sites to the substrate and diffusion of the epoxide back to the reaction bulk. It was observed that all the LDH-based catalytic materials needed 24 h for improved and stable epoxide production to be achieved, indicating that the products were initially adsorbed on the LDH-based catalytic materials and slowly released into solution. To check whether the products were really adsorbed onto the LDH matrixes, the reactions were repeated for 24 and 48 h and an extraction process was conducted. It involved adding 200 μL aliquots of the reaction solvent to the solid LDH-based catalytic material obtained at the end of the reaction, withdrawing each aliquot, and placing the removed aliquot in a flask until a total volume of 10.0 mL of extract was obtained. The products were analyzed again, to notice 14 to 15% extra epoxide yield for all the reactions after the extraction (see Fig. 7). All the reactions were selective to the epoxide, which was the sole product: the surface basicity of the hydrotalcite has been suggested to have an advantage in

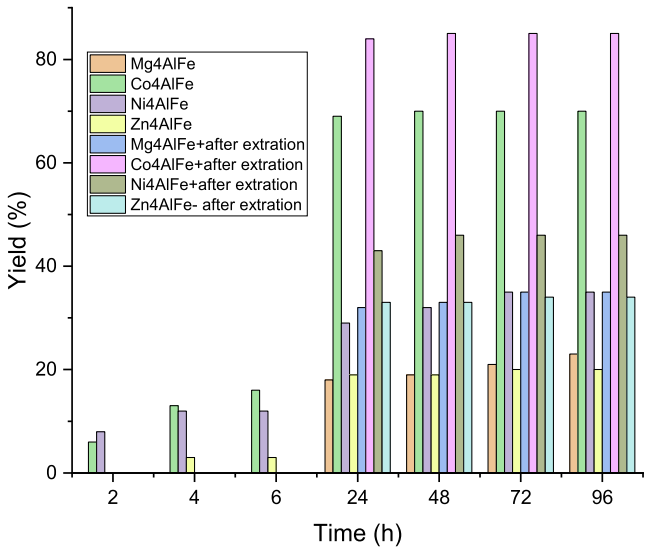

Fig. 7. Oxidation of cyclooctene using heat-treated catalysts and extraction of products from solids.

the epoxidation of olefins (Dai et al., 2020). The epoxide yields obtained followed the descending order, Co_4AlFe, Ni_4AlFe, Mg_4AlFe, and Zn_4AlFe, with LDH-based Co_4AlFe giving 85 % total epoxide yield (that is, the sum of 70% epoxide of the initial analysis with the additional 15% obtained after the extraction procedure), which was similar to results previously reported by our group (Saltarelli et al., 2019) employing as catalyst an aminoiron(III) porphyrin immobilized on an alumina matrix prepared by the sol–gel non-hydrolytic route; the reaction under similar conditions gave 87% epoxide yield after 24 h. This similarity allowed us to infer that iron ions in LDH played an essential role in catalysis. Indeed, taking a look at Table 5, the sample with higher surface iron content also gave better catalytic results for the epoxidation reaction (85% yield). It should be also noted that the double bond oxidation to epoxides is favored by transition metals that are able to adopt high oxidation states as demonstrated by Wentzel et al. (1998, 2000, 2004) which could help us to understand the good performance of Co_4AlFe sample. Indeed, the LDH present similar characteristic to a previous system prepared by the non-hydrolytic sol–gel process (Caetano et al., 2006) and involving the high-valent oxo-metal species $Co^{IV} = O$ as the most probable active species in this transfer, for cobalt aluminum silicate complexes. In fact, these systems could present a combined effect of two catalytic active sites – iron(III) and cobalt(III) – leading to a mechanism that resembles the cytochrome *P*-450 mechanism. The epoxidation mechanism comprises two steps: the first step generates the $Co^{IV} = O$ species via two-electron oxidation of the tetrahedral Co^{2+} ions or one-electron oxidation of octahedral Co^{3+} ions by iodosylbenzene; in the second step, the $Co^{IV} = O$ species transfer the oxygen atom to the epoxide carbon–carbon double bond, to form the epoxide. The combined mechanisms proposed for epoxidation of olefins with Co_3O_4 and Fe_3O_4 systems involves the coordination of the oxidant to the metal center. The Lewis acidity of the Co or Fe center could increase the oxidizing power of the metal-oxo group, as previously reported by Askarinejad et al. (2010). These authors verify that nanosized cobalt ions present a higher catalytic activity, the LDH induce the site isolation of Co and Fe active sites, mimicking biological enzymes. It should be also emphasized that, as previously discussed on TPR section, Fig. 5, the Co and Fe redox mechanism described for LDH-based Co_4AlFe was proven to be compatible with the metal-oxo mechanism.

To prove that catalysis was genuinely heterogeneous, the LDH-based catalytic materials were filtered (with and without heat-treatment) off the reaction mixture, then extra oxidant was added to the resulting supernatant, and the oxidation reaction allowed to proceed under the same

initial conditions for another 96 h. After this period, no cyclooctene oxide yields were detected, indicating that the catalytic activity of the LDH-based catalytic materials was truly heterogeneous, and that metals played an essential role in catalysis.

The stability of the catalysts prepared herein was confirmed via catalyst reuse. For this purpose, the solid catalysts were separated from the reaction mixture after each experiment by simple filtration, according to the procedure described in the experimental part, and dried before being used in a subsequent run. In all cases the catalyst was reused in three consecutive runs without any decrease in catalytic performance.

4. Conclusion

Aluminum recovered from saline slags originated in the aluminum recycling industry was used to succesfully synthesize layered double hydroxides. All the samples contained iron and aluminum as M^{3+} and different divalent cations. Their capacity as catalysts for the oxidation of cyclooctene was tested to evaluate their biomimetic potential. Results highlight the great potential of these catalysts, which obtained a yield up to 85% and great selectivity to the epoxide (100 %), a sought after intermediate in chemical industries. The iron present in the surface of the solids was responsible for their performances and its combination with the divalent cations gave diverse results attributed to their redox mechanism. Thus, reaction yields followed the descending order Co_4AlFe, Zn_4AlFe, Ni_4AlFe, and Mg_4AlFe. This advanced LDH show major improvements not only by reducing the production costs but specially by giving a new life to a hazardous waste that was bound to finish in landfills and cause a water and soil contamination issue.

CRediT authorship contribution statement

L. Santamaría: Conceptualization, Methodology, Writing – original draft, Investigation, Writing – review & editing. **L. Oliveira García:** Investigation. **E.H. de Faria:** Investigation. **K.J. Ciuffi:** Conceptualization, Investigation, Supervision, Writing – review & editing. **M.A. Vicente:** Supervision, Writing – review & editing. **S.A. Korili:** Supervision, Writing – review & editing. **A. Gil:** Conceptualization, Methodology, Writing – original draft, Supervision, Writing – review & editing.

Declaration of Competing Interest

The authors declare that they have no known competing financial interests or personal relationships that could have appeared to influence the work reported in this paper.

Acknowledgements

This work was funded by the Spanish Ministry of Science and Innovation (MCIN/AEI/10.13039/501100011033) through project PID2020-112656RB-C21. The Brazilian authors thank Conselho Nacional de Desenvolvimento Científico e Tecnológico (CNPq) and the Brazilian research funding agency Fundação de Amparo à Pesquisa do Estado de São Paulo (FAPESP) (2020/06712-6). Open access funding provided by Universidad Pública de Navarra. LS thanks the Universidad Pública de Navarra for a post-doctoral grant. AG also thanks Banco Santander for funding through the Research Intensification Program.

References

Ahmed, A.A.A., Talib, Z.A., Hussein, M.Z.B., Zakaria, A., 2012. Improvement of the crystallinity and photocatalytic property of zinc oxide as calcination product of Zn-Al layered double hydroxide. J. Alloys Compd. 539, 154–160. https://doi.org/10.1016/j.jallcom.2012.05.093.

Antonangelo, A.R., Grazia Bezzu, C., Mughal, S.S., Malewschik, T., McKeown, N.B., Nakagaki, S., 2017. A porphyrin-based microporous network polymer that acts as an efficient catalyst for cyclooctene and cyclohexane oxidation under mild conditions. Catal. Commun. 99, 100–104. https://doi.org/10.1016/j.catcom.2017.05.024.

Asif, M., Aziz, A., Azeem, M., Wang, Z., Ashraf, G., Xiao, F., Chen, X., Liu, H., 2018. A review on electrochemical biosensing platform based on layered double hydroxides for small molecule biomarkers determination. Adv. Colloid Interface Sci. 262, 21–38. https://doi.org/10.1016/j.cis.2018.11.001.

Askarinejad, A., Bagherzadeh, M., Morsali, A., 2010. Catalytic performance of Mn_3O_4 and Co_3O_4 nanocrystals prepared by sonochemical method in epoxidation of styrene and cyclooctene. Appl. Surf. Sci. 256, 6678–6682. https://doi.org/10.1016/j.apsusc.2010.04.069.

Bizaia, N., De Faria, E.H., Ricci, G.P., Calefi, P.S., Nassar, E.J., Castro, K.A.D.F., Nakagaki, S., Ciuffi, K.J., Trujillano, R., Vicente, M.A., Gil, A., Korili, S.A., 2009. Porphyrin-kaolinite as efficient catalyst for oxidation reactions. ACS Appl. Mater. Interfaces 1, 2667–2678. https://doi.org/10.1021/am900556b.

Caetano, B.L., Rocha, L.A., Molina, E., Rocha, Z.N., Ricci, G., Calefi, P.S., de Lima, O.J., Mello, C., Nassar, E.J., Ciuffi, K.J., 2006. Cobalt aluminum silicate complexes prepared by the non-hydrolytic sol-gel route and their catalytic activity in hydrocarbon oxidation. Appl. Catal. A Gen. 311, 122–134. https://doi.org/10.1016/j.apcata.2006.06.028.

Cavani, F., Trifirò, F., Vaccari, A., 1991. Hydrotalcite-type anionic clays: Preparation, properties and applications. Catal. Today 11, 173–301. https://doi.org/10.1016/0920-5861(91)80068-K.

Chagas, L.H., De Carvalho, G.S.G., Do Carmo, W.R., San Gil, R.A.S., Chiaro, S.S.X., Leitão, A.A., Diniz, R., De Sena, L.A., Achete, C.A., 2015. MgCoAl and NiCoAl LDHs synthesized by the hydrothermal urea hydrolysis method: Structural characterization and thermal decomposition. Mater. Res. Bull. 64, 207–215. https://doi.org/10.1016/j.materresbull.2014.12.062.

Dai, X., Huang, J., Tang, S., Zheng, X., Jiang, O., Peng, X., 2020. Efficient aerobic epoxidation of olefins accelerated by a bifunctional Co2Al layered double hydroxide. React. Kinet. Mech. Catal. 131, 283–296. https://doi.org/10.1007/s11144-020-01867-9.

El Hassani, K., Kalnina, D., Turks, M., Beakou, B.H., Anouar, A., 2019. Enhanced degradation of an azo dye by catalytic ozonation over Ni-containing layered double hydroxide nanocatalyst. Sep. Purif. Technol. 210, 764–774. https://doi.org/10.1016/j.seppur.2018.08.074.

European Commission, 2014. 2014/955/EU: Commission Decision of 18 December 2014 amending Decision 2000/532/EC on the list of waste pursuant to Directive 2008/98/EC of the European Parliament and of the Council Text with EEA relevance. Off. J. Eur. Union 7, 44–86.

Fernández, J.M., Ulibarri, M.Á., M. Labajos, F., Rives, V., 1998. The effect of iron on the crystalline phases formed upon thermal decomposition of Mg-Al-Fe hydrotalcites. J. Mater. Chem. 8, 2507–2514. https://doi.org/10.1039/A804867C.

Gil, A., 2005. Management of the Salt Cake from Secondary Aluminum Fusion Processes. Ind. Eng. Chem. Res. 44, 8852–8857. https://doi.org/10.1021/ie050835o.

Gil, A., Korili, S.A., 2016. Management and valorization of aluminum saline slags: Current status and future trends. Chem. Eng. J. 289, 74–84. https://doi.org/10.1016/j.cej.2015.12.069.

Greenwood, N.N., Earnshaw, A., 1997. Chemistry of the Elements –, Second edition. Butterworth-Heinemann.

Groves, J.T., 2006. High-valent iron in chemical and biological oxidations. J. Inorg. Biochem. 100, 434–447. https://doi.org/10.1016/j.jinorgbio.2006.01.012.

Hadnadjev-Kostic, M., Vulic, T., Ranogajec, J., Marinkovic-Neducin, R., Radosavljevic-Mihajlovic, A., 2013. Thermal and photocatalytic behavior of Ti/LDH nanocomposites. J. Therm. Anal. Calorim. 111, 1155–1162. https://doi.org/10.1007/s10973-012-2226-5.

Hernández, W.Y., Aliç, F., Verberckmoes, A., Van Der Voort, P., 2017. Tuning the acidic–basic properties by Zn-substitution in Mg–Al hydrotalcites as optimal catalysts for the aldol condensation reaction. J. Mater. Sci. 52, 628–642. https://doi.org/10.1007/s10853-016-0360-3.

Javali, S., Chandrashekar, A.R., Naganna, S.R., Manu, D.S., Hiremath, P., Preethi, H.G., Vinod Kumar, N., 2017. Eco-concrete for sustainability: utilizing aluminium dross and iron slag as partial replacement materials. Clean Technol. Environ. Policy 19, 2291–2304. https://doi.org/10.1007/s10098-017-1419-9.

Jawad, A., Peng, L., Liao, Z., Zhou, Z., Shahzad, A., Ifthikar, J., Zhao, M., Chen, Z., Chen, Z., 2019. Selective removal of heavy metals by hydrotalcites as adsorbents in diverse wastewater: Different intercalated anions with different mechanisms. J. Clean. Prod. 211, 1112–1126. https://doi.org/10.1016/j.jclepro.2018.11.234.

Kapoor, M.P., Matsumura, Y., 2004. Liquid-phase methanol carbonylation catalyzed over tin promoted nickel-aluminium layered double hydroxide. Catal. Today 93–95, 287–291. https://doi.org/10.1016/j.cattod.2004.06.059.

Kirm, I., Medina, F., Rodríguez, X., Cesteros, Y., Salagre, P., Sueiras, J., 2004. Epoxidation of styrene with hydrogen peroxide using hydrotalcites as heterogeneous catalysts. Appl. Catal. A Gen. 272, 175–185. https://doi.org/10.1016/j.apcata.2004.05.039.

Lee, S Bin, Ko, E.H., Park, J.Y., Oh, J.M., 2021. Mixed metal oxide by calcination of layered double hydroxide: Parameters affecting specific surface area. Nanomaterials 11, 1–19. https://doi.org/10.3390/nano11051153.

Li, F., Duan, X., 2005. Applications of layered double hydroxides. Struct. Bond. 119, 193–223. https://doi.org/10.1007/430_007.

Li, Q., Meng, M., Tsubaki, N., Li, X., Li, Z., Xie, Y., Hu, T., Zhang, J., 2009. Performance of K-promoted hydrotalcite-derived CoMgAlO catalysts used for soot combustion, NOx storage and simultaneous soot-NOx removal. Appl. Catal. B Environ. 91, 406–415. https://doi.org/10.1016/j.apcatb.2009.06.007.

Lin, Y., Maghool, F., Arulrajah, A., Horpibulsuk, S., 2021. Engineering characteristics and environmental risks of utilizing recycled aluminum salt slag and recycled concrete as

a sustainable geomaterial. Sustainability 13, 10633. https://doi.org/10.3390/su131910633.

Lucas, H.J., Kennedy, E.R., Forno, M.W., 1963. Iodosobenzene Diacetate. Org. Synth. 43, 62. https://doi.org/10.15227/orgsyn.043.0062.

Misol, A., Jiménez, A., Morato, A., Labajos, F.M., Rives, V., 2020. Quantification by Powder X-ray Diffraction of Metal Oxides Segregation During Formation of Layered Double Hydroxides. Eur. J. Eng. Res. Sci. 5, 1243–1248. https://doi.org/10.24018/ejers.2020.5.10.2192.

Murayama, N., Maekawa, I., Ushiro, H., Miyoshi, T., Shibata, J., Valix, M., 2012. Synthesis of various layered double hydroxides using aluminum dross generated in aluminum recycling process. Int. J. Miner. Process. 110–111, 46–52. https://doi.org/10.1016/j.minpro.2012.03.011.

Naseem, S., Gevers, B., Boldt, R., Labuschagné, F.J.W.J., Leuteritz, A., 2019. Comparison of transition metal (Fe Co, Ni, Cu, and Zn) containing tri-metal layered double hydroxides (LDHs) prepared by urea hydrolysis. RSC Adv. 9, 3030–3040. https://doi.org/10.1039/c8ra10165e.

Parida, K., Satpathy, M., Mohapatra, L., 2012. Incorporation of Fe^{3+} into Mg/Al layered double hydroxide framework: Effects on textural properties and photocatalytic activity for H_2 generation. J. Mater. Chem. 22, 7350–7357. https://doi.org/10.1039/c2jm15658j.

Qiu, Z., Tai, C.W., Niklasson, G.A., Edvinsson, T., 2019. Direct observation of active catalyst surface phases and the effect of dynamic self-optimization in NiFe-layered double hydroxides for alkaline water splitting. Energy Environ. Sci. 12, 572–581. https://doi.org/10.1039/c8ee03282c.

Rives, V., Prieto, O., Dubey, A., Kannan, S., 2003. Synergistic effect in the hydroxylation of phenol over CoNiAl ternary hydrotalcites. J. Catal. 220, 161–171. https://doi.org/10.1016/S0021-9517(03)00245-8.

Saltarelli, M., de Faria, E.H., Ciuffi, K.J., Nassar, E.J., Trujillano, R., Rives, V., Vicente, M. A., 2019. Aminoiron(III)–porphyrin–alumina catalyst obtained by non-hydrolytic sol-gel process for heterogeneous oxidation of hydrocarbons. Mol. Catal. 462, 114–125. https://doi.org/10.1016/j.mcat.2018.09.014.

Santamaría, L., Devred, F., Gaigneaux, E.M., Vicente, M.A., Korili, S.A., Gil, A., 2020a. Effect of the surface properties of Me2+/Al layered double hydroxides synthesized from aluminum saline slag wastes on the adsorption removal of drugs. Micropor. Mesopor. Mater. 309 https://doi.org/10.1016/j.micromeso.2020.110560.

Santamaría, L., Korili, S.A., Gil, A., 2022. Layered double hydroxides from slags: Closing the loop. J. Environ. Chem. Eng. 10 https://doi.org/10.1016/j.jece.2021.106948.

Santamaría, L., López-Aizpún, M., García-Padial, M., Vicente, M.A., Korili, S.A., Gil, A., 2020b. Zn-Ti-Al layered double hydroxides synthesized from aluminum saline slag wastes as efficient drug adsorbents. Appl. Clay Sci. 187 https://doi.org/10.1016/j.clay.2020.105486.

Sharefkin, J.G., Saltzmann, H., 1963. Iodosobenzene. Org. Synth. 43, 60. https://doi.org/10.15227/orgsyn.043.0060.

Trujillano, R., Nájera, C., Rives, V., 2020. Activity in the Photodegradation of 4-Nitrophenol of a Zn, Al Hydrotalcite-Like Solid and the Derived Alumina-Supported ZnO. Catalysts 10, 702. https://doi.org/10.3390/catal10060702.

Webb, P.A., Orr, C., 1997. Analytical methods in fine particle technology. Micromeritics Instrument Corporation.

Wentzel, B., A. Gosling, P., C. Feiters, M., J. M. Nolte, R., 1998. Mechanistic studies on the epoxidation of alkenes with molecular oxygen and aldehydes catalysed by transition metal–β-diketonate complexes. J. Chem. Soc. Dalt. Trans. 2241–2246. https://doi.org/10.1039/A801175C.

Wentzel, B.B., Alsters, P.L., Feiters, M.C., Nolte, R.J.M., 2004. Mechanistic Studies on the Mukaiyama Epoxidation. J. Org. Chem. 69, 3453–3464. https://doi.org/10.1021/jo030345a.

Wentzel, B.B., Leinenen, S.M., Thomson, S., Sherrington, D.C., Fetters, M.C., Nolte, R.J. M., 2000. Aerobic epoxidation of alkenes using polymer-bound Mukaiyama catalysts. J. Chem. Soc. Perkin Trans. 1, 3428–3431. https://doi.org/10.1039/b005066k.

Yoldi, M., Fuentes-Ordoñez, E.G., Korili, S.A., Gil, A., 2019. Efficient recovery of aluminum from saline slag wastes. Miner. Eng. 140 https://doi.org/10.1016/j.mineng.2019.105884.